**Title**
Specification of x-ray mirrors in terms of system performance: new twist to an old plot



**Journal**
Optical Engineering, 54(2)

**ISSN**
0091-3286

**Authors**
Yashchuk, Valeriy V
Samoylova, Liubov V
Kozhevnikov, Igor V

**Publication Date**
2015-02-09

**DOI**
10.1117/1.oe.54.2.025108

Peer reviewed

Optical Engineering

OpticalEngineering.SPIEDigitalLibrary.org

# Specification of x-ray mirrors in terms of system performance: new twist to an old plot

Valeriy V. Yashchuk
Liubov V. Samoylova
Igor V. Kozhevnikov

SPIE.

# Specification of x-ray mirrors in terms of system performance: new twist to an old plot

**Valeriy V. Yashchuk,[a,*] Liubov V. Samoylova,[b] and Igor V. Kozhevnikov[c]**
[a]Lawrence Berkeley National Laboratory, 1 Cyclotron Road, Berkeley, California 94720, United States
[b]European XFEL GmbH, Albert-Einstein-Ring 19, 22761 Hamburg, Germany
[c]Russian Academy of Sciences, Shubnikov Institute of Crystallography, Leninsky pr., 59, 119333 Moscow, Russia

**Abstract.** In the early 1990s, Church and Takacs pointed out that the specification of surface figure and finish of x-ray mirrors must be based on their performance in the beamline optical system. We demonstrate the limitations of specification, characterization, and performance evaluation based on conventional statistical approaches, including root-mean-square roughness and residual slope variation, evaluated over spatial frequency bandwidths that are system specific, and a more refined description of the surface morphology based on the power spectral density distribution. We show that these limitations are fatal, especially in the case of highly collimated coherent x-ray beams, like beams from x-ray free electron lasers (XFELs). The limitations arise due to the deterministic character of the surface profile data for a definite mirror, while the specific correlation properties of the surface are essential for the performance of the entire x-ray optical system. As a possible way to overcome the problem, we treat a method, suggested by Yashchuk and Yashchuk in 2012, based on an autoregressive moving average modeling of the slope measurements with a limited number of parameters. The effectiveness of the approach is demonstrated with an example specific to the x-ray optical systems under design at the European XFEL.  [DOI: 10.1117/1.OE.54.2.025108]

Keywords: x-ray optics; surface metrology; specification; simulation; surface finish and figure; power spectral density; autoregressive moving average; fabrication tolerances.

Paper 141691P received Oct. 31, 2014; accepted for publication Jan. 7, 2015; published online Feb. 9, 2015.

## 1 Introduction

The unique properties of modern synchrotron radiation sources and x-ray free electron lasers (XFELs), including their high flux and brightness, and, in the case of XFEL, high coherence and time resolution, make them indispensable tools in the exploration in physics, chemistry, biology, and material science. Delivery of the brightness of the x-ray sources to the sample, nanofocusing, and coherence preservation rely on the availability of x-ray optics of unprecedented quality with surface slope accuracy <0.15 $\mu$rad and surface height error of <1 nm.[1–5] During the last few years, significant progress on the fabrication of such high-quality x-ray optics has been achieved.[6–12]

The uniqueness of the optics and the limited number of proficient vendors makes the fabrication of state-of-the-art x-ray optics extremely time consuming and expensive. It is, therefore, essential to provide the specifications for optical fabrication exactly as is numerically evaluated to be adequate for the required beamline performance, avoiding overspecification as well as underspecification. The numerical simulation of the performance of optics for new beamlines and those under upgrade requires refined and reliable information about the expected surface slope and height distributions of the planned x-ray optics before they are fabricated. Such information should be based on metrology data from existing mirrors, fabricated by the same vendor and technology, but may have different desired sizes, as well as slope and height root-mean-square (rms) variations.

*Address all correspondence to: Valeriy V. Yashchuk, E-mail: VVYashchuk@lbl.gov

When the performance of an optical system is reliably described by the geometrical optics, the use of ray tracing methods[13–19] allows evaluation of the effect of lower spatial frequency errors of optical surfaces usually given with residual slope distributions after subtraction of the desired surface shape (surface figure). A powerful approach to evaluate the effects of surface imperfection with middle and high spatial frequencies (surface finish) to the performance of x-ray optical systems consists of sophisticated x-ray scattering (diffraction) calculations based on the one- or two-dimensional (1-D or 2-D) power spectral density (PSD) distribution of the surface height, allowing for the evaluation of three-dimensional distributions of x-rays scattered by the optics.[20–30]

In the early 1990s, Church and Takacs pointed out that the specification of surface figure and finish of x-ray mirrors must be based on their imaging performance, and the results can be expressed in terms of statistical quantities, such as rms roughness and residual slope variation, that are directly accessible from optical metrology.[23,24] The spatial frequency bandwidths of applicability of geometrical and diffraction optics are determined by the radiation source and beamline system parameters rather than by the metrology instruments. To estimate the error parameters over the bandwidth related to the system performance, the PSD spectra measured with bandwidth-limited instruments are extrapolated to the wanted frequency range by fitting an analytical model, such as an inverse power law (fractal) spectral distribution.[31,32] The PSD extrapolation is more reliable when based on PSD measurements performed with different instruments providing different but, preferably, overlapping spatial frequency ranges.[33–37] The found, extrapolated, modeled PSD spectrum is used (via inversed Fourier transform) for the simulation of

metrology data for x-ray optics before fabrication and prediction of the performance of the optical system.[27–30]

In the present work, we investigate the applicability of the PSD-based evaluation of beamline performance of prospective x-ray optics for XFELs, for the case when dedicated optical systems deliver the beams over distances of hundreds of meters. The conclusion is that in this case, the PSD-based specification is not sufficient. Here, we suggest a recipe for a more refined analysis of the expected beamline performance of x-ray optics before fabrication and provide an example of the application of the analysis to an optic under design for one of the beamlines of the European XFEL.

This paper is organized as follows. In Sec. 2, we analyze the effect of mirror surface error at different spatial frequencies on the quality of x-ray beams delivered to the sample position. To the best of our knowledge, we are the first to claim that trustworthy estimations of expected performance of prospective optics for XFEL applications must also include evaluation of the expected dispersion of the performance, which can be very large. In Sec. 3, we apply autoregressive moving average (ARMA) modeling[38,39] to the surface slope error distribution measured with a high-quality mirror. Based on the determined ARMA model, we generate many surface height traces that are used in Sec. 4 to numerically simulate performance and estimate the performance dispersion of an XFEL optic under design. The paper concludes (Sec. 5) by summarizing the main concepts discussed.

## 2 Effect of Mirror Residual Error on Beam Quality

### 2.1 *Limitations of Current Specification of Mirror Quality as Applied to XFEL Beamlines*

The simplest way to estimate the mirror quality consists of a separation of the surface relief errors into two types: surface figure and finish errors. The figure error, or surface waviness, implies long-scale deviations of the mirror surface shape $z = z(x)$ from the ideal one resulting in the appearance of slope errors $\mu(x)$. In the geometrical optics approximation, the slope errors cause a beam deflection from the desired direction of propagation with a consequent widening of the focused spot size. The natural condition of the reflective surface quality is that the deflected rays fall onto a sample inside the focused spot of angular size $\Psi$ seen from the mirror surface:

$$\mu < \Psi/2. \tag{1}$$

The finish error is determined by the small-scale microroughness and gives rise to diffuse scattering. The angular width of the scattered radiation depends on the correlation length of roughness and, as a rule, essentially exceeds the angle $\Psi$ in Eq. (1). Therefore, the necessary condition of the surface smoothness requires the total integrated scattering to be as small as possible and the rms roughness to satisfy the following condition (see, for example, Refs. 40 and 41):

$$\sigma < \lambda/(4\pi \sin\theta), \tag{2}$$

where $\lambda$ is the radiation wavelength and $\theta$ is the grazing incident angle. The separation of the optical surface error onto the figure and finish errors in this manner is a matter of convention. Equations (1) and (2) give no way to quantitatively estimate the degradation of imaging or focusing due to waviness or roughness.

A more consistent estimation of the necessary mirror quality was performed by Church and Takacs.[23,24] Basing on a semiempirical relation for the radiation intensity distribution in the image plane and assuming the coherence length of the incident beam along the mirror surface to be much less than its geometrical length, they derived an expression for the on-axis Strehl factor:

$$\frac{I(0)}{I_0(0)} \approx 1 - \frac{8}{\Theta^2}\mu^2 - \left(\frac{4\pi\sigma}{\lambda}\sin\theta\right)^2, \tag{3}$$

where $\Theta$ is the angular size of the image, and $\sigma$ and $\mu$ are the rms roughness and the rms residual slope error, as in Eqs. (1) and (2). The values of $\sigma$ and $\mu$ are determined over the spatial frequency intervals, specific for the optic's application. The slope error is determined in the range of low frequencies, i.e., for long-scale surface inhomogeneities exceeding the coherence length of the incident beam, while the roughness is determined in the range of high frequencies. The on-axis Strehl factor is only the ratio of the on-axis image intensity in the presence of errors to its value for zero errors. Derivation of Eq. (3) is based on the description of the reflective surface with a PSD function rather than an *a priori* separation of the surface shape errors onto the figure and finish errors. Nevertheless, such a separation is assumed: surface features with the length exceeding the radiation coherence length reflect the incident wave according to the geometrical optics laws [the surface slope error term in Eq. (3)], while the small-scale roughness effect is estimated based on the diffraction theory [the surface roughness term in Eq. (3)].

Equation (3) is acceptable to characterize the quality of mirrors used with incoherent sources. In these applications, blurring of the image or focal spot is one of the most crucial distortions.

In XFEL beamline applications, an estimation of the mirror quality with Eq. (3) is insufficient.

First, one of the main applications of XFELs is for different diffraction experiments to measure and analyze diffraction patterns from a sample with a goal to reconstruct its internal structure. Therefore, high-performing x-ray mirrors have to be able to preserve the wave front of the incident radiation inside the focused spot on the sample. Deviation of the mirror surface from an ideal one results in the appearance of scattered waves, which, after interference with the unperturbed wave, form speckles (irregularities of the radiation intensity caused by irregularities of the wave front) inside the beam spot (Sec. 4). The speckles make analysis of the diffraction pattern very hard, if at all possible. Even though Eq. (1) is obeyed, i.e., all deflected rays are inside the focused spot, the mirror may not be of high enough quality for XFEL applications. Therefore, the Strehl ratio is of little importance for XFEL mirror specification.

Second, XFEL radiation is totally transversely coherent, and thus, separation of surface irregularities into surface figure and finish errors makes no sense for XFEL mirrors.

Third, the XFEL radiation divergence is only several microradians, and, correspondingly, the source-to-mirror, $r_0$, and the mirror-to-sample, $r_1$, distances range up several hundred meters. As a result, the mirror surface errors at the longest spatial wavelengths, comparable with the mirror

length, have the greatest effect on the quality of the reflected beam. This fact imposes rigid requirements on the XFEL mirrors.

As an example, let us consider the self-amplified spontaneous emission (SASE1) beamline at the European XFEL (see Sec. 4), where $r_0 \approx 300$ m and $r_1 \approx 600$ m. The divergence of radiation with $\lambda = 0.1$ nm is as small as $\delta\theta \approx 2$ $\mu$rad, and the grazing angle of the incident radiation is $\theta_0 \approx 2$ mrad. The light reflection scheme is shown in Fig. 1.

The spatial frequency components, $\nu_x$ and $\nu_y$, responsible for radiation scattering in the direction $\theta$ and $\varphi$ are determined from the following diffraction equation:

$$\nu_x = \frac{1}{\lambda}|\cos\theta - \cos\theta_0| \approx \frac{1}{\lambda}\theta_0\Delta\theta,$$
$$\Delta\theta = |\theta - \theta_0|,$$
$$\nu_y = \frac{1}{\lambda}\cos\theta_0 \sin\varphi \approx \frac{1}{\lambda}\varphi. \tag{4}$$

If $S$ is the linear size of the focusing spot on the sample, its angular size, seen from the mirror surface, is $S/r_1$. The spatial frequencies responsible for scattering radiation inside the spot (damaging frequencies) are determined by the conditions $\Delta\theta < S/(2r_1)$ and $\varphi < S/(2r_1)$; therefore,

$$\nu_x < \frac{S\theta_0}{2r_1\lambda}; \qquad \nu_y < \frac{S}{2r_1\lambda}. \tag{5}$$

Generally, the spot size $S$ depends on a number of parameters, such as the focal length of the mirror, distances $r_0$ and $r_1$, incidence angle $\theta_0$. In the case of a flat mirror, neglecting the finite size of the beam on the exit aperture of the source, $S \approx (r_0 + r_1)\delta\theta$. Then Eq. (5) gives

$$\nu_x < \frac{\theta_0\delta\theta}{2\lambda}\left(1 + \frac{r_0}{r_1}\right); \qquad \nu_y < \frac{\delta\theta}{2\lambda}\left(1 + \frac{r_0}{r_1}\right). \tag{6}$$

Equation (6) sets the upper limit of the damaging frequencies. By convention, we can also introduce a lower limit, which is determined by the (inverse) size of the beam on the mirror surface $S' \approx r_0\delta\theta$; then

$$\nu_x > \frac{\theta_0}{r_0\delta\theta}; \qquad \nu_y > \frac{1}{r_0\delta\theta}. \tag{7}$$

With the parameters of the SASE1 beamline at the European XFEL, the ranges of spatial frequencies, which can bring speckles into existence, are $\nu_x \sim 0.033$ to 0.3 cm$^{-1}$ and $\nu_y \sim 16.5$ to 150 mm$^{-1}$. These frequencies correspond to the spatial lengths $d_x \sim 3.3$ to 30 cm and $d_y \sim 6.7$ to 60 $\mu$m.

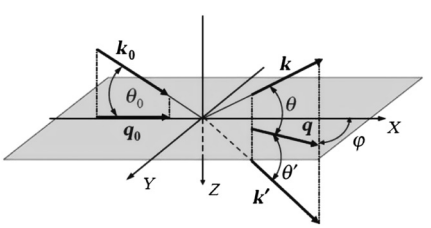


**Fig. 1** Diffraction scheme used for the estimation of the spatial frequency range, important for x-ray free electron laser (XFEL) mirror specification.

Suppose that there is a mirror surface irregularity with the characteristic length $\xi$. It brings to the reflected wave front a feature with the length of $\xi \sin\theta_0$. At the distance $R$ from the mirror due to diffraction, the feature is widened to $\lambda R/(\xi \sin\theta_0)$. If the distance $R$ is large enough, $R \gg (\xi \sin\theta_0)^2/\lambda$, the feature on the wave front disappears. Substituting $\lambda = 0.1$ nm, $\theta_0 \approx 2$ mrad, and the irregularity length on the mirror surface $\xi = 10$ cm, one finds that the corresponding perturbation feature on the wave front disappears at the distance $R \gg 200$ m, which is comparable with the characteristic lengths of the SASE1 beamline. At the same time, a feature due to a surface irregularity with the length $\xi = 1$ cm disappears after the distance $R \gg 2$ m.

The spatial lengths of surface irregularities along the $Y$ axis are shorter by three to four orders of magnitude as compared with those along the $X$ axis. Such irregularities do not give rise to speckles on the sample placed at several hundred meters from the mirror.

Therefore, at XFELs, the quality of the reflected beam is mostly affected by long surface irregularities, comparable with the mirror length. Below, we discuss the problems of specification of mirrors for the beamlines under design based on existing surface metrology data.

### 2.2 *Statistical Limitations of Measured Power Spectral Densities at Lower Spatial Frequencies*

Interpretation and use of surface metrology data corresponding to the spatial wavelength of the order of the mirror length are closely related to a general problem of spectral analysis known as the problem of statistical stability of data.[42] In short, for a single limited realization (one mirror with a finite length and a measurement with discrete sampling), one can only make an estimation of the PSD. The poor statistical stability of the estimated PSD spectrum is seen as intense fluctuation from frequency to frequency and from realization to realization (from mirror to mirror).

Figure 2 presents the experimental surface slope data for the Linac Coherent Light Source (LCLS) beam split and delay mirror.[43] The residual (after subtraction of the best-fit third-order polynomial) slope variation over the mirror clear aperture of 138 mm [Fig. 2(a)] was measured with the Advanced Light Source (ALS) developmental long trace profiler (DLTP).[44] The DLTP is capable of slope metrology of plane surfaces with an absolute error better than 80 nrad and with an rms error of <50 nrad.[45,46] The overall error of the present data is estimated to be <60 nrad (rms).[47] The corresponding PSD, calculated as a square of digital Fourier transform of the slope distribution, is shown in Fig. 2(b) with a solid, strongly varying line. The variation at the lower spatial frequencies reached almost two orders of magnitude.

The statistical stability of measured PSD spectra can be improved with additional measurements over significantly separated surface subareas that are statistically uncorrelated. Averaging over the corresponding PSDs suppresses the spectral fluctuations, usually at the medium and higher spatial frequencies. This approach to increase statistical stability of the measured PSD at the lower spatial frequencies does not work for grazing incidence x-ray optics, when the mirror length is much larger than its width. In this case, surface metrology, performed over the entire optical clear aperture, provides only a single realization of the mirror profile, which can be used for estimation of the PSD spectrum. Statistically

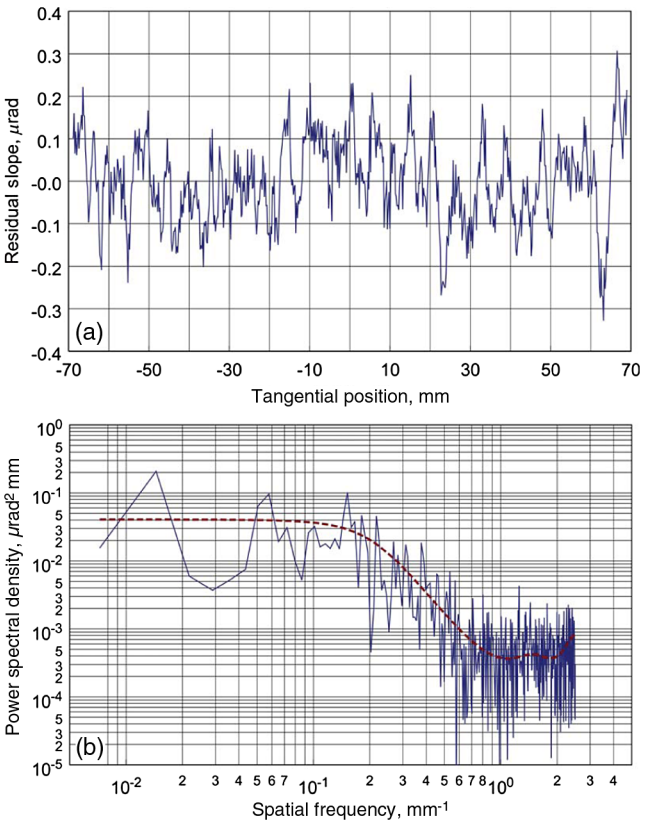


**Fig. 2** (a) Measured residual (after subtraction of the best-fit third-order polynomial) slope variation of the linac coherent light source (LCLS) beam split and delay mirror. (b) The power spectral density calculated via digital Fourier transform of the slope distribution (the blue solid line) and the analytical power spectral density (PSD) corresponding to the autoregressive moving average (ARMA) model, discussed in Sec. 3. The slope variation data in plot (a) are used throughout the paper as the basis for the ARMA modeling of the data used for the European x-ray free electron laser (XFEL) self-amplified spontaneous emission (SASE1) beamline performance simulations. The white-noise-like asymptotical behavior of the measured PSD distribution at the higher spatial frequencies corresponds to the random noise of the developmental long trace profiler measurements of ~40 nrad [root mean square (rms)]. The frequency cut-off relates to the instrumental resolution of ~1.7 mm,[38,39,48] characteristic for an autocollimator-based profilometer with an aperture with diameter of 2.5 mm. The tangential position increment of 0.2 mm, used for the measurements, suggests significant oversampling. The oversampling is useful for precise lateral matching and averaging of the measurement runs performed at different experimental arrangements.[46]

uncorrelated measurements can only be made with different x-ray optics fabricated with the same technology and, hopefully, possessing the same statistical properties. This is usually impossible because of the uniqueness of the optics.

If the statistically unstable (unique) data are used for simulation of beamline performance of x-ray optics before fabrication (and are, therefore, different from the measured ones), one should expect a strong uncertainty of the simulation results.

In Refs. 38 and 39, a method for highly reliable forecasting of the expected surface slope distributions of the prospective x-ray optics has been suggested and demonstrated (see discussion in Sec. 3). The method is based on an ARMA modeling of the slope measurements with a limited number of parameters. With the found parameters, the surface slope profile of an optic with the newly desired specification can be forecast. ARMA modeling also provides an analytical expression for the PSD, which can be thought of as a result of averaging over PSDs of an infinite number of different realizations of the profiles described with the same model. In Fig. 2(b), such an analytically calculated PSD of the LCLS beam split and delay mirror is shown with a dashed red line. Variation of the measured PSD around the analytical one gives a way to estimate the dispersion of the measured scattered light intensity, as discussed in Sec. 4.

The problem of statistical instability of metrology data at lower spatial frequencies is closely related to the problem in the prediction of results of measurements of scattered light intensity, considered below.

### 2.3 *Problem of the Prediction of Light Scattering from a Surface of the Finite Size*

In this section, we discuss shortly one more fundamental reason that does not allow faithful prediction of the light intensity scattered from a surface of finite size.

Let us consider scattering of an x-ray beam, limited in the transverse direction, by a flat rough surface with the height error function $z(\vec{\rho})$, $\vec{\rho} \equiv (x, y)$ and analyze only the flux scattered outside the focal spot, ignoring the interference of the scattered light with the unperturbed wave (Fig. 1). This problem is analogous to the one considered in Refs. 23 and 24.

In the first-order perturbation theory of the height roughness, the angular distribution of the scattered radiation, $\Phi_L(\theta, \varphi)$, is expressed as (see, for example, Refs. 25 and 49)

$$\Phi_L(\theta,\varphi) \equiv \frac{1}{Q_{\text{inc}}}\frac{dQ_{\text{scat}}}{d\Omega} = \frac{A(\theta,\varphi)}{L^2}\int_{L^2} z(\vec{\rho}_1)z(\vec{\rho}_2)\exp[i(\vec{q}_0-\vec{q})(\vec{\rho}_1-\vec{\rho}_2)]\mathrm{d}^2\vec{\rho}_1\mathrm{d}^2\vec{\rho}_2, \tag{8}$$

where $dQ_{\text{scat}}$ is the radiation power, scattered into the solid angle $\delta\Omega = \cos\theta \cdot \delta\theta\delta\varphi$ and normalized to the incident power $Q_{\text{inc}}$, $L^2$ is the size of the illuminated area on the surface, and $A(\theta, \varphi)$ is a factor that depends on the incidence and scattering angles, the radiation wavelength, and the dielectric permittivity of the surface material, while it is independent of $z(\vec{\rho})$.

If the surface profile $z(\vec{\rho})$ is known, the scattering pattern can be calculated via Eq. (8). However, our goal is to predict the scattered intensity distribution in the case when the averaged statistical properties of the surface error $z(\vec{\rho})$, described with its PSD function, are all that is known.

First, assume that the surface is infinite in space and that the PSD function of the surface height error, $z(\vec{\rho})$, is known at all spatial frequencies from zero to infinity. By tending the size of the illuminated area to infinity, one obtains, from Eq. (8), the average scattering distribution as a function of the PSD of the surface error:

$$\Phi(\theta,\varphi) \equiv \lim_{L\to\infty}\Phi_L(\theta,\varphi) = A(\theta,\varphi)\cdot \mathrm{PSD}_{2D}(\vec{\nu}), \tag{9}$$

where $2\pi\vec{\nu} = \vec{q}_0 - \vec{q}$ (see Fig. 1). Equation (9) defines a deterministic function determined for any spatial frequency, even extremely small ones.

If the surface error obeys the ergodic property,[50] spatial averaging is equivalent to an ensemble one. The scattering

distribution, averaged over an ensemble of limited size surfaces with identical statistical properties, is also a deterministic function:

$$\langle \Phi_L(\theta,\varphi)\rangle = \frac{A(\theta,\varphi)}{L^2}\int \mathrm{PSD}_{2D}(\vec{\nu}) \times \left\{\frac{\sin[(\Delta q_x - 2\pi\nu_x)L/2]}{(\Delta q_x - 2\pi\nu_x)/2}\cdot\frac{\sin[(\Delta q_y - 2\pi\nu_y)L/2]}{(\Delta q_y - 2\pi\nu_y)/2}\right\}^2 \mathrm{d}^2\vec{\nu}; \quad \Delta\vec{q} \equiv \vec{q} - \vec{q}_0, \tag{10}$$

which allows calculation of the averaged angular distribution of scattering from a single mirror if the PSD function is known at all spatial frequencies.

Note that

$$\langle \Phi_L(\theta,\varphi)\rangle \neq \Phi(\theta,\varphi). \tag{11}$$

The scattering distribution [Eq. (8)] from each of the limited-size surfaces is a random function. In order to reliably predict the scattering distribution from a single surface, one should estimate the difference (dispersion) expected between the scattering distribution [Eq. (8)] and the scattering averaged over the whole ensemble [Eq. (10)]. The dispersion of the scattered flux is

$$D[\Phi_L(\theta,\varphi)] \equiv \sqrt{\langle \Phi_L^2(\theta,\varphi)\rangle - \langle \Phi_L(\theta,\varphi)\rangle^2}. \tag{12}$$

A meaningful prediction of the scattering distribution is only possible if the dispersion of the flux is small compared to its mean value [Eq. (10)]: $D[\Phi_L(\theta,\varphi)] \ll \langle \Phi_L(\theta,\varphi)\rangle$.

References 22 and 51 provide an estimation of the relative dispersion of the flux scattered into a small solid angle $\delta\Omega$:

$$\frac{D[\Phi_L(\theta,\varphi)]}{\langle \Phi_L(\theta,\varphi)\rangle} \sim \left(\frac{\lambda^2}{L^2 \sin\theta_0 \delta\Omega}\right)^{1/2}. \tag{13}$$

Equation (13) is valid if the relative dispersion of the flux is small and does not exceed unity. In the limiting case $\delta\Omega \to 0$, the flux dispersion tends to the finite value[51]

$$\frac{D[\Phi_L(\theta,\varphi)]}{\langle \Phi_L(\theta,\varphi)\rangle} \to \sqrt{1 + \left[\frac{\sin(\Delta q_x L)}{\Delta q_x L}\cdot\frac{\sin(\Delta q_y L)}{\Delta q_y L}\right]^2}. \tag{14}$$

From Eq. (13), the dispersion tends to zero with increasing size of the illuminated area $L^2$. Equation (13) also suggests that the more accurately we want to predict scattering (or the smaller the value of $\delta\Omega$), the higher is the statistical uncertainty, caused by the finite size of the mirror.

Equation (13) does not contain in an explicit form the correlation length $\xi$ of the surface irregularities. However, if we are interested in the details of the angular distribution of the scattered flux, we should make the values of $\delta\theta$ and $\delta\varphi$ far less (by a factor of $M \gg 1$) than the angular width of the scattering pattern in both directions. Then, from Eq. (13), we obtain

$$\frac{D[\Phi_L(\theta,\varphi)]}{\langle \Phi_L(\theta,\varphi)\rangle} \sim M\frac{\xi}{L}. \tag{15}$$

According to Eq. (15), the dispersion of the scattered flux is extremely small when the effect of microroughness ($\xi \ll L$) to the scattering pattern is analyzed. In this case, the surface averaging of the flux [Eq. (8)] provides a faithful prediction of the angular distribution of the scattered light.

If the effect of very long surface irregularities, comparable with the mirror length ($\xi \sim L$), is of interest, even the total (integrated) scattered flux ($M = 1$) cannot be truthfully predicted. This is because the dispersion of the scattered flux appears to be on the order of the mean value of the flux.

Therefore, a valid prediction of the scattering caused by long-scale surface irregularities, whose length is comparable with the length of the mirror (important for performance evaluation of XFEL beamlines under design), must include both the evaluation of the averaged scattered flux distribution and its dispersion. Below, we suggest a recipe for such an evaluation.

## 3 Autoregressive Moving Average Modeling and Forecasting of Slope Metrology with the LCLS Beam Split Mirror

### 3.1 *Brief Review of ARMA Modeling*

Let us consider 1-D surface slope metrology with high-quality x-ray optics. The result of the metrology is a distribution (trace) of residual (after subtraction of the best-fit figure and trends) slopes $\alpha[n]$ measured over discrete points $x_n = n\cdot\Delta x$ ($n = 1,\ldots,N$), where $N$ is the total number of observations, and $(N-1)\Delta x$ is the total length of the trace, uniformly, with an increment $\Delta x$, distributed along the trace.

ARMA modeling describes the discrete surface slope distribution $\alpha[n]$ as a result of a uniform stochastic process:[42,50]

$$\alpha[n] = \sum_{l=1}^{p} a_l \alpha[n-l] + \sum_{l=0}^{q} b_l \eta[n-l], \tag{16}$$

where $\eta[n]$ is zero-mean unit-variance white Gaussian noise (to make shorter: white Gaussian noise), which is the driving noise of the model. The parameters $p$ and $q$ are the orders of the autoregressive and moving average processes, respectively. At $q = 0$ and $b_0 = 1$, the ARMA process [Eq. (16)] reduces to an AR stochastic process. In addition to the linearity, the ARMA transformation is time-invariant since its coefficients depend on the relative lags, $l$, rather than on $n$. The goal of the modeling is to determine the ARMA orders and estimate the corresponding AR and MA coefficients $a_l$ and $b_l$.[52–54]

ARMA fitting allows for the replacement of the spectral estimation problem by a problem of parameter estimation. When an ARMA model is identified, the corresponding PSD distribution can be analytically derived:[42]

$$P_h(f) = \sigma^2 \frac{B[e^{i2\pi f}]B[e^{-i2\pi f}]}{A[e^{i2\pi f}]A[e^{-i2\pi f}]}, \tag{17}$$

where the frequency $f \in [-0.5, 0.5]$,

$$A[e^{i2\pi f}] = 1 + a_1 e^{i2\pi f} + \ldots + a_p e^{i2\pi p f}, \tag{18}$$

$$B[e^{i2\pi f}] = b_0 + b_1 e^{i2\pi f} + \ldots + b_q e^{i2\pi q f}. \tag{19}$$

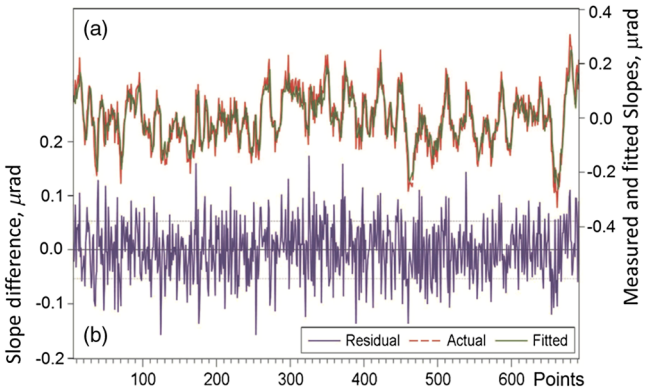


**Fig. 3** (a) Measured slope trace (the red dashed line) after subtracting the best-fitted third polynomial shape in order to remove the trend that is characteristic for short x-ray mirrors, and best-fitted slope trace (the green solid line), corresponding to the ARMA model specified in Table 1. The rms variation of the measured slope trace is 0.0993 $\mu$rad. (b) Difference between the measured and fitted traces. The rms variation of the slope difference is 0.0529 $\mu$rad.

Equation (17) can be expressed as

$$P_x(f)=\sigma^2\frac{(b_0+b_1z^{-1}+\ldots+b_qz^{-q})(b_0+b_1z^{1}+\ldots+b_qz^{q})}{(1-a_1z^{-1}-\ldots-a_pz^{-p})(1-a_1z^{1}-\ldots-a_pz^{p})}, \tag{20}$$

where $z=e^{i2\pi f}$ and $\sigma^2$ is the variance of the driving noise $\eta[n]$.

Therefore, a low-order ARMA fit, if successful, allows parameterization of the PSD of a random rough surface. As a result, the PSD distributions appear as highly smoothed versions of the corresponding estimates via a direct digital Fourier transform.[38,39] Description of a rough surface as the result of an ARMA stochastic process provides a model-based mechanism for extrapolating the spectra outside the measured bandwidth.[38,39] Recent publications[38,39,55,56] describe a successful application of ARMA modeling to the experimental surface slope data for a 1280 m spherical reference mirror.[57,58] In the next section, we apply ARMA modeling to the results of slope metrology with the mirror, shown in Fig. 2.

### 3.2 *ARMA Fitting of Slope Measurements with the LCLS Beam Split and Delay Mirror*

For determining the ARMA model parameters and verifying the statistical reliability of the model, we use a commercially available software package EViews 8.[59,60]

Figure 3 reproduces the measured residual slope trace, shown with the red dashed line. The trace consists of $N=691$ points measured with an increment of $\Delta x=0.2$ mm.

The best-fitted slope trace, shown with the green solid line, corresponds to the ARMA model specified in Table 1. The table, generated by EViews 8 software as the regression output, includes only the ARMA parameters found to be statistically significant. As can be seen by the low probabilities and the high $t$ statistics in the regression output above, AR(1), AR(2), AR(5), and MA(2) coefficients are highly statistically significant at <1% significance level.

The regression output, generated by EViews software (Table 1), contains the results of the application of several methods helpful for evaluation of the reliability of the regression output. The regression describes 72% of the data's

**Table 1** Parameters of the autoregressive moving average model [the green solid line in Fig. 3(a)], which best fits the surface slope trace for the LCLS beam split and delay mirror measured with the ALS developmental long trace profiler. In Eqs. (16)–(20), $b_0=1$ and $\sigma$ is equal to the standard error (S.E.) of the regression of 0.0529 $\mu$rad (root mean square). The data in the table are the regression outputs generated by EViews 8 software.

| Dependent variable: SLOPE | | | | |
|---|---|---|---|---|
| Method: least squares | | | | |
| Included observations: 686 after adjustments | | | | |
| Convergence achieved after five iterations | | | | |
| Variable | Coefficient | S.E. | *t* statistic | Prob. |
| AR(1): $a_1$ | 0.636773 | 0.036423 | 17.48286 | 0.0000 |
| AR(2): $a_2$ | 0.351020 | 0.040657 | 8.633774 | 0.0000 |
| AR(5): $a_5$ | −0.147487 | 0.026652 | −5.533809 | 0.0000 |
| MA(2): $b_2$ | −0.065918 | 0.003542 | −18.61053 | 0.0000 |
| *R*-squared | 0.716945 | Mean dependent variation | | −8.01E − 10 |
| Adjusted *R*-squared | 0.715700 | S.D. dependent variation | | 9.92E − 08 |
| S.E. of regression | 5.29E − 08 | Akaike info criterion | | −30.66587 |
| Sum squared residuals | 1.91E − 12 | Schwarz criterion | | −30.63945 |
| Log likelihood | 10522.39 | Hannan-Quinn criterion | | −30.65564 |
| Durbin-Watson statistics | 2.008293 | | | |

variance, as indicated with the value of $R^2 \approx 0.72$. The Durbin-Watson statistic, a test for first-order serial correlation of the residuals, is ~2, suggesting that there is no serial correlation. EViews also reports various informational criteria that are helpful as a model selection guide, for example, when examining the number of regression lags.[42,60]

The slope difference trace shown in Fig. 3(b) is the driving noise of the model $\eta[n]$ in Eq. (16) and should be distinguished from any observation noise or measurement error. According to the ARMA definition, the driving noise must be normally distributed. Figure 4 reproduces the results of EViews' normality test for the residuals. Together with other criteria, the low Jarque-Bera statistic[60] and the high probability indicate that the values of the slope difference are normally distributed.

### 3.3 *ARMA Forecasting of Surface Topography of Statistically Identical SASE1 Offset Mirrors with 800 mm Length*

The ARMA modeling of the existing metrology data provides a natural approach for forecasting the quality of the optics before fabrication. The forecasting is based on the assumption that a certain polishing process at the particular fabrication facility is uniquely parameterized with its ARMA model, determined from the measurements with a prefabricated mirror. The question of uniqueness is out of the scope of this article.

Forecasting a prospective optic with the determined ARMA model is performed in two steps. First, we generate a new sequence of white-noise-like, normally distributed residuals $\eta[n]$ with an appropriate slope error variance, $\sigma^2$, and with the length of the sequence corresponding to the desired mirror length. Second, by using Eq. (16) with the determined ARMA parameters, as those in Table 1, and the extended residuals, an optical surface with the prescribed properties is generated.

In order to estimate the expected dispersion of the beamline performance of the optic via wave front propagation simulation, discussed in Sec. 4, a number of statistically independent forecasts are needed. For this, uncorrelated sets of white-noise-like residuals (over the entire profile length) are generated and used to forecast statistically identical (with the predetermined ARMA parameters), but generally uncorrelated (due to the uncorrelated residuals $\eta[n]$) optics.

Figure 5 presents four slope distributions, forecast based on the ARMA model (Table 1), established for the LCLS beam split and delay mirror. The distributions with the rms slope error of 0.1 $\mu$rad have the overall length of 800 mm (with 0.2 mm increment), as specified for the European XFEL SASE1 flat offset mirror under performance simulation (Sec. 4). As the driving residuals $\eta[n]$, we used white noise traces with a total number of $N = 4001$ points generated with the EViews 8 software.[59,60]

The statistical identity of the generated slope traces to the used ARMA model was verified by ARMA modeling the traces with EViews 8 in a manner similar to that described in Sec. 3.2. Within the statistical uncertainty, the parameters of the ARMA models, identified for the generated slope traces, are equal to those of the ARMA model of the measured slope trace (see Table 1).

Figure 6 shows the surface height distributions, obtained as a running sum of the corresponding slope distributions (Fig. 5).

Unlike the rms variations of the slope traces, the rms and the peak-to-valley variations of the height distributions have a significant variation. This is expected. Indeed, from the derivative theorem[42] that connects the Fourier transformations of a function and its derivative, the 1-D PSD function, $\mathrm{PSD}_\alpha(f)$, of a slope distribution $\alpha(x)$ and the 1-D PSD function, $\mathrm{PSD}_z(f)$, of the corresponding height distribution, $z(x)$, are related as

$$\mathrm{PSD}_z(f) = (2\pi f)^{-2}\mathrm{PSD}_\alpha(f), \tag{21}$$

where $f$ is the spatial frequency. The multiplier $(2\pi f)^{-2}$ in Eq. (21) effectively enhances the fluctuation of the $\mathrm{PSD}_z(f)$ at the lower spatial frequency range.

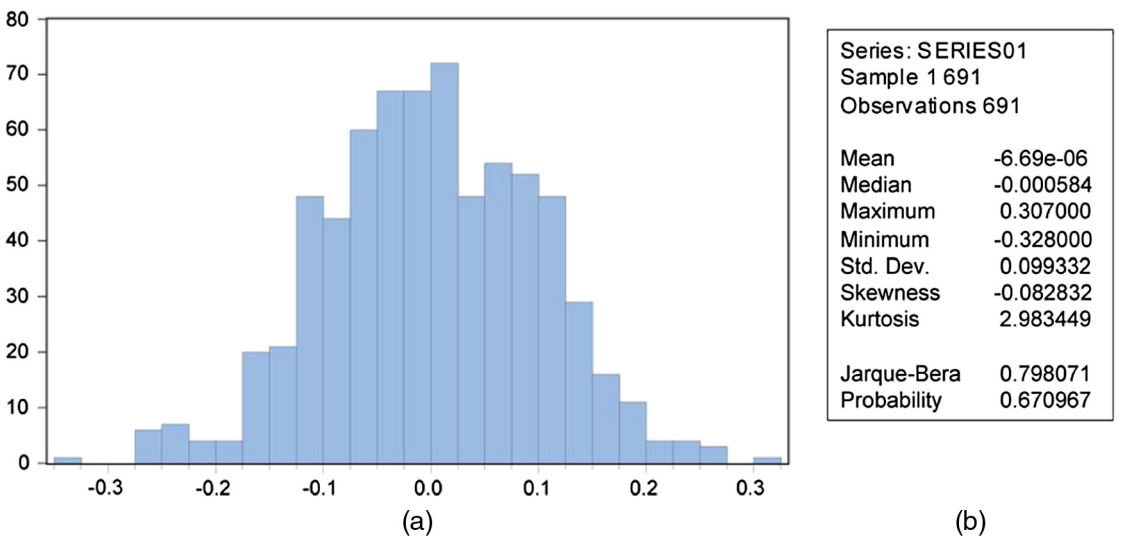


**Fig. 4** Histogram normality test[60] for the slope difference of the regression shown in Fig. 3. (a) Histogram of the values of the slope difference. (b) Descriptive statistics of the values, including the Jarque-Bera statistic used for testing whether the values are normally distributed. All the descriptive statistics indicate that the slope difference is normally distributed.

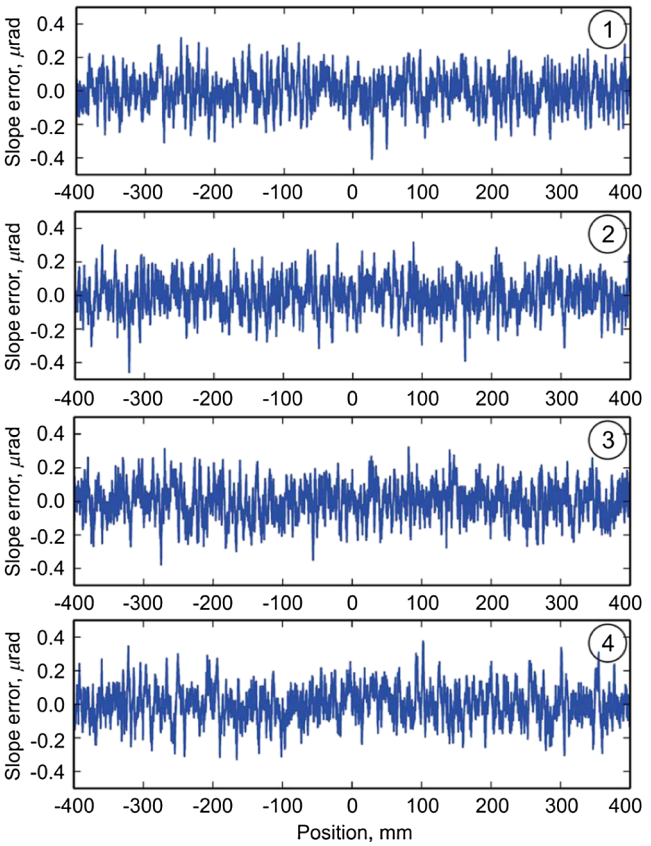


**Fig. 5** Slope error traces with the length of 800 mm, generated with the ARMA model specified in Table 1. The rms slope variation of 0.1 $\mu$rad is the same for all traces. Because of the same model parameters used to generate the distributions, the PSD spectra of the traces are also identical.

## 4 Performance Simulation of SASE1 Beamline with Forecast Height Distributions

The unprecedented photon flux and spatial coherence of FEL sources makes single particle imaging feasible. In particular, the macromolecular complexes and single biomolecules are typically some tens of nanometers in size and are mainly composed of light chemical elements (carbon, nitrogen, oxygen). The x-ray scattering from such an object is very weak, and maximizing the single pulse photon flux delivered to the sample is critical for this class of experiments.[61] This requirement imposes the constraint that the x-ray optics used to focus and deliver the XFEL beam to the sample must be highly transmissive, with the largest fraction of the beam being delivered to the interaction region in a focal spot comparable to the size of the sample.

In order to demonstrate the effect of the dispersion of metrology data on beamline performance, we treat as a real-life example the case of European XFEL SASE1 beamline and consider the results of numerical simulations for one of the experimental stations.

### 4.1 *European XFEL SASE1 Beamline Arrangement*

The European XFEL in Hamburg will deliver coherent x-ray pulses with femtosecond duration and high repetition rate up to 4.5 MHz.[62] There will be two hard x-ray and one soft x-ray undulator sources based on SASE. The lengths of hard x-ray beamlines exceed 900 m. Figure 7 shows the layout of the

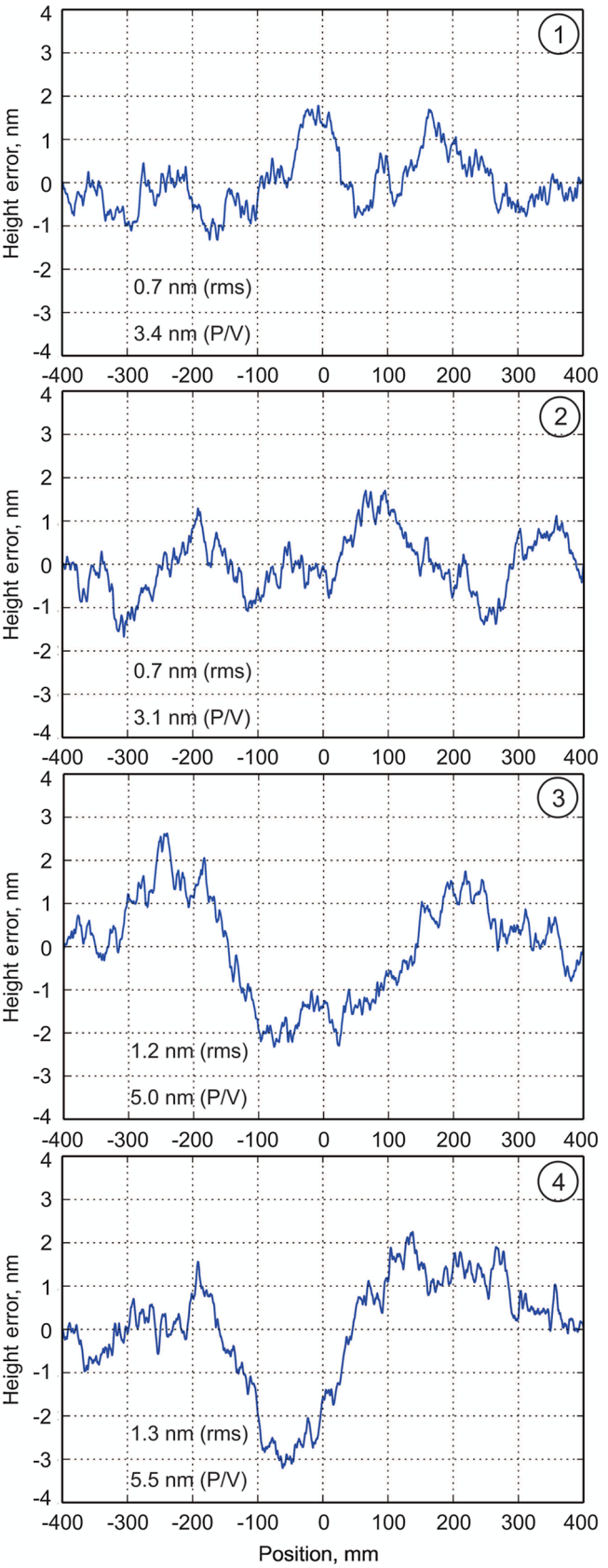


**Fig. 6** Height error traces with a length of 800 mm, obtained as a running sum of the corresponding slope distributions in Fig. 5. The values of the rms and the peak-to-valley height variations are presented on the corresponding plots. Numbers in the circles identify the forecast slope profile in Fig. 5, used for simulation of the corresponding height distribution.

single particle and bioimaging instrument at the European XFEL hard x-ray SASE1 beamline that includes two offset mirrors and a Kirkpatrick-Baez (KB) system of horizontal and vertical mirrors (focusing distance 3.0 and 1.9 m, respectively), focusing the XFEL beam to a submicrometer spot.[61] For the modeling discussed below, a simplified scheme consisting of a flat offset mirror, at a distance of 246 m from the source, and the KB mirror system located 654 m downstream of the offset mirror is used. The offset mirror is assumed to be the only optic in the beamline that has a surface profile error predicted by the ARMA model described in Sec. 3. The KB mirrors are assumed to be ideally shaped without any surface error. At the incidence angle of 3.5 mrad, the mirror aperture perpendicular to the beam propagation direction is 3.2 mm, accepting $4\sigma$ of the XFEL beam.

### 4.2 *Simulation Results*

For wave front propagation simulation, the Synchrotron Radiation Workshop library[63] and WavePropaGator framework[64] were used. The code is based on the Fourier optics approach and optical elements are presented as a set of propagators. For modeling the impact of the mirror surface errors, a phase screen with wave front distortions $\exp[-(2\pi/\lambda)2z(x)\sin\theta]$ at an offset mirror position was introduced,[65] where $2\pi/\lambda$ is the wave vector, $z(x)$ is the height error profile, and $\theta$ is the incidence angle.

Simulation results are shown in Figs. 8 and 9. The profiles with the same value of rms slope error cause different speckle-like patterns on the KB entrance aperture (Fig. 8). They also have different impacts on the focal spot quality (Fig. 9) and transmission (relative to the ideal mirror) of the system that varies from 69 to 89% for slope distributions 1 and 4, respectively (Fig. 5).

The simulation results in Fig. 9 suggest that the beam quality is sufficient for slope distributions 1 to 3, but inacceptable for distribution 4, when two focal spots and a significant decrease of photon flux density are observed. This illustrates the conclusion formulated in Sec. 2.3: for surface irregularities with the length comparable with the length of the mirror, which have a main impact on the XFEL beam quality, the scattered flux dispersion is the same order of value as the averaged flux. Note that the same is true when the mirror is directly specified in the height domain (rather than in the slope domain).

## 5 Discussion and Conclusions

Any mirror used in XFEL beamlines is a unique optical element with extremely high quality of the reflecting surface and with a length up to 1 m or more. The uniqueness and extraordinary high cost of the mirrors dictate a strong necessity for very careful specification of the optical surface fabrication tolerances and selection of the most suitable fabrication technology and vendor. These should be based on thorough simulation and analysis of the expected beamline performance of the mirror using all available information about the quality of existing mirrors fabricated with the most prominent polishing technologies.

The problems of prediction of the mirror quality before fabrication and appropriate usage of the prediction for the performance evaluation are the major topics investigated in the present paper.

A very informative characteristic of the scattering properties of a mirror is the PSD function describing statistical properties of the surface irregularities in the spatial frequency domain. We have analyzed applicability of the PSD-based evaluation of beamline performance of prospective (before fabrication) x-ray optics for XFELs, when dedicated optical systems deliver the highly collimated coherent x-ray beams over distances of hundreds of meters. We have shown that in this case, the classical specification based on the PSD of a surface error distribution, measured with a single existing mirror, is not applicable. In the XFEL case, the mirror surface errors at the longer spatial wavelengths, comparable with the mirror length, have the greatest effect on the quality of the reflected beam, leading to the appearance of speckles in the focal plane. In this respect, we have pointed out two fundamental problems. First, the stability of measured PSD spectra of existing mirrors at longer spatial wavelengths is unavoidably poor. This is associated with an unavoidably large error in the determination from a single measurement of the corresponding PSD function. Second, a truthful prediction of the scattering caused by long-scale surface irregularities appears to be impossible, even though the PSD is known exactly at all spatial frequencies, because the dispersion of the scattered flux was demonstrated to be of the order of the flux mean value. Therefore, the only way to predict the future mirror quality is the use of a probabilistic approach, i.e., determination of the mathematical expectation to fabricate a mirror that provides the

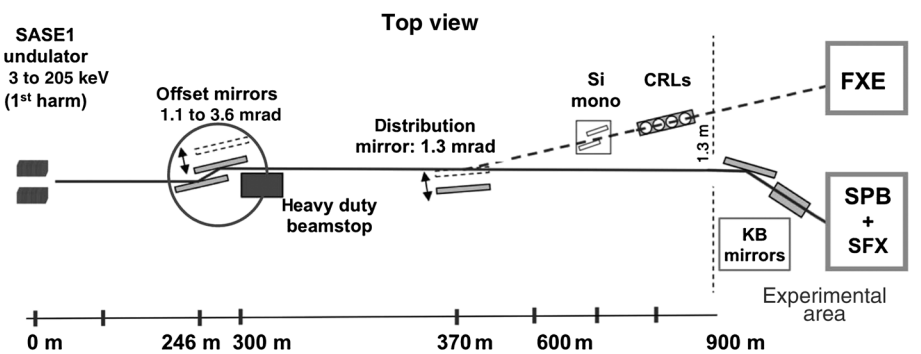


**Fig. 7** The optical scheme of thte single particle and bioimaging (SPB) instrument at European XFEL SASE1 beamline: the SPB layout includes two offset mirrors at distances 246 and 258 m, and a 100-nm-scale focusing Kirkpatrick-Baez (KB) system of horizontal and vertical mirrors with focusing distances 3 and 1.9 m, respectively.[61] The KB entrance aperture is at 929.6 m, with incidence angle at 3.5 mrad.

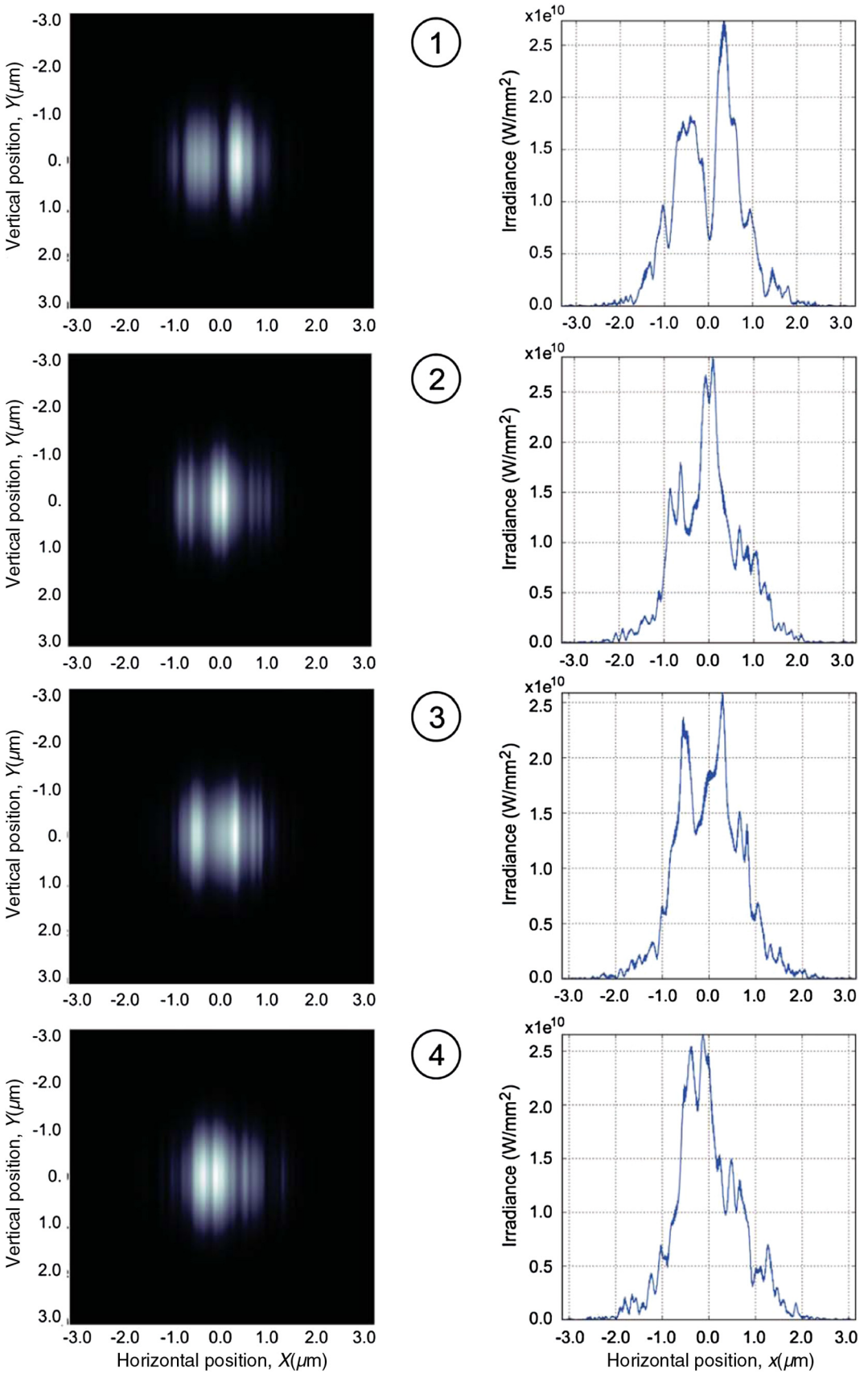


**Fig. 8** Simulated distributions of light irradiance on the entrance aperture of the KB mirror system at 929.6 m from the source: two-dimensional (2-D) distributions (the left-hand set of images) and cross-sections of the 2-D distributions in the horizontal direction at near the vertical position $Y = 0.0$ mm (the right-hand set of plots). Numbers in the circles identify the forecast slope profile (Fig. 5), used for simulation of the corresponding distribution of light irradiance.

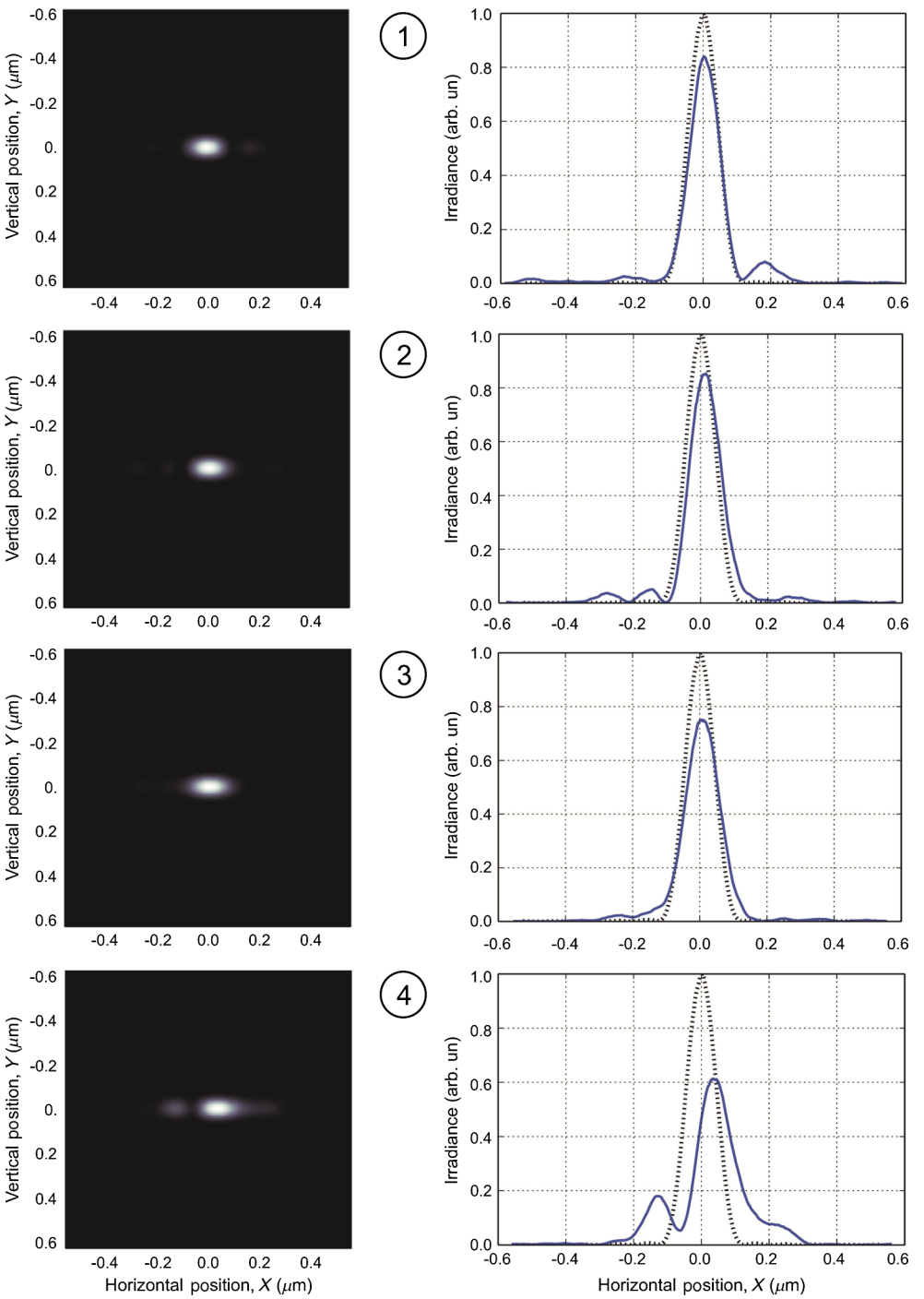


**Fig. 9** Simulated distributions of light irradiance in the focal plane at 932.6 m from the source: 2-D distributions (the left-hand set of images) and cross-sections of the 2-D distributions in the horizontal direction at near the vertical position $Y = 0.0$ $\mu$m (the right-hand set of plots). The dotted lines in the plots correspond to the ideal surface of the mirror under investigation. Numbers in the circles identify the forecast slope profile (Fig. 5), used for simulation of the corresponding distribution of light irradiance.

peak-to-valley value of the radiation irregularities on the sample surface lower than the required one.

To the best of our knowledge, we are the first to claim that the trustworthy performance estimations (and corresponding optical specification) should include evaluation of the dispersion of the performance, associated with inherent poor stability of measured PSD spectra at shorter spatial wavelengths.

We have suggested a recipe for the required refined analysis of the expected beamline performance and dispersion of the performance of prospective x-ray optics. The idea is to generate a set of trustful surface error distributions that would mimic many mirrors, fabricated by the same vendor and technology as used for fabrication of the existing prototype optic.

For modeling and parameterization of the measured residual surface slope errors of the prototype optic, we employ the method recently suggested and demonstrated in Refs. 38 and 39. The method is based on an ARMA modeling of the polished surface, considered as a result of a

uniform stochastic process. The ARMA model determined for the prototype optics is used to forecast a set of new surface error distributions with the same statistical properties (inherent PSD), but with a different distribution length.

We have applied the suggested recipe to numerically simulate beamline performance of a flat offset mirror under design for use in the SASE1 beamline of the European XFEL.

As a prototype, a high-quality beam split and delay mirror fabricated for the LCLS is considered. The measured rms residual slope variation of the LCLS mirror is 0.1 $\mu$rad, and the length of the mirror clear aperture is 138 mm. The specified length of the SASE1 offset mirror under simulation is 800 mm. Using a commercially available software package, we have established the best-fit ARMA model of the LCLS mirror. The determined ARMA model has only four statistically significant AR and MA parameters. Based on the model, many surface slope traces that have 0.1 $\mu$rad rms surface slope error and length of 800 mm were generated. The surface height distributions needed for the simulations were obtained as a running sum of the generated slope distributions.

The generated surface height distributions have been used for performance simulation of the prospective SASE1 flat offset mirrors. Simulation results have shown that the height profiles with the same value of rms slope error cause very different speckle-like patterns on the KB entrance aperture. The impact of different height profiles on the focal spot quality is also very different. Depending on the used trace, the transmission of the SASE 1 optical system varies by a factor of ~1.5. This is in spite of the fact that the distributions are statistically identical (having the same rms slope variation and the same inherent PSD). Variation of the beam quality in the focus also has a strong variation. With some generated height distributions, it is even not acceptable for the beamline application, having two focal spots and a significant decrease in photon flux density.

On the whole, the performed investigations totally support the major point of this paper about the importance of evaluation of the dispersion of the optical performance in order to get trustworthy performance estimations and, therefore, reasonable specification of the x-ray optics for the XFEL beamlines under development.

With the obvious success and perspective of the application of 1-D ARMA modeling and forecasting, more rigorous beamline performance simulation requires highly reliable methods to model and forecast 2-D surface topography. As a possible solution, time-invariant linear filter (TILF) based approximation of surface metrology data has been considered in Refs. 55 and 56 as a natural extension of ARMA modeling. TILF modeling allows a direct, straightforward generalization to 2-D random fields. Mathematical foundations of the generalization are well established.[66] However, its practical realization requires development of calculation algorithms and dedicated software for determining the optimal TILF best fitted to the measured 2-D surface slope and height distributions and for forecasting new distributions.

The forthcoming investigations must also solve the question about the uniqueness of the ARMA and TILF parameterizations for the state-of-the-art polishing processes used for fabrication of x-ray optics. This can be performed, for example, by cross-comparing the ARMA and TILF models for different optics which are identically fabricated. The archived metrology data for high-quality x-ray optics, collected at synchrotron facilities around the world, could be used.

In conclusion, we would like to cite the following from Ref. 22: "Parametric statistics, which make use of models, lead to the greatest economy of description, but lead to the temptation of using them in regions, where their validity may be unknown. ... The development of physically-based wide-band surface models is a critical problem in the field of surface measurement and characterization." This was said 30 years ago. And we hope that our current investigation adds a new, and hopefully, useful twist to this old plot.

## Acknowledgments

The authors are very grateful to Wayne R. McKinney for very useful discussions and to Daniel J. Merthe, Nikolay A. Artemiev, and Daniele Cocco for help with high-accuracy surface slope measurements of the LCLS beam split and delay mirror. The Advanced Light Source is supported by the Director, Office of Science, Office of Basic Energy Sciences, Material Science Division of the U.S. Department of Energy under Contract No. DE-AC02-05CH11231 at Lawrence Berkeley National Laboratory. One of the authors (I.V.K.) was supported by the Russian Ministry of Science and Education via the program "Physics at the accelerators and reactors of the West Europe (excluding CERN)."

## References

1. D. Mills and H. Padmore, "X-ray optics for BES light source facilities," 2013, http://science.energy.gov/~/media/bes/pdf/reports/files/BES_XRay_Optics_rpt.pdf.
2. S. Moeller et al., "Photon beamlines and diagnostics at LCLS," *Nucl. Instrum. Methods Phys. Res. A* **635**(1), S6–S11 (2011).
3. S. Roling et al., "Time-dependent wave front propagation simulation of a hard x-ray split-and-delay unit: towards a measurement of the temporal coherence properties of x-ray free electron lasers," *Phys. Rev. ST Accel. Beams* **17**, 110705 (2014).
4. N. Kelez et al., "Design of an elliptically bent refocus mirror for the MERLIN beamline at the advanced light source," *Nucl. Instrum. Methods Phys. Res. A* **582**(01), 135–137 (2007).
5. K. Yamauchi et al., "Wave-optical analysis of sub-micron focusing of hard x-ray beams by reflective optics," *Proc. SPIE* **4782**, 271–276 (2002).
6. K. Yamauchi et al., "Figuring with sub-nanometer-level accuracy by numerically controlled elastic emission machining," *Rev. Sci. Instrum.* **73**(11), 4028–4033 (2002).
7. C. Liu et al., "From flat substrate to elliptical KB mirror by profile coating," *AIP Conf. Proc.* **705**(01), 704–707 (2004).
8. F. Siewert et al., "Advanced metrology: an essential support for the surface finishing of high performance x-ray optics," *Proc. SPIE* **5921**, 592101 (2005).
9. A. Schindler et al., "Finishing procedure for high performance synchrotron optics," *Proc. SPIE* **5180**, 64–72 (2003).
10. M. Kanaoka et al., "Figuring and smoothing capabilities of elastic emission machining for low-thermal-expansion glass optics," *J. Vac. Sci. Technol. B* **25**(06), 2110–2113 (2007).
11. T. Arnold et al., "Ultra-precision surface finishing by ion beam and plasma jet techniques: status and outlook," *Nucl. Instrum. Methods Phys. Res. A* **616**(2–3), 147–156 (2010).
12. H. Thiess, H. Lasser, and F. Siewert, "Fabrication of x-ray mirrors for synchrotron applications," *Nucl. Instrum. Methods Phys. Res. A* **616**(2–3), 157–161 (2010).
13. M. S. del Río et al., "SHADOW3: a new version of the synchrotron x-ray optics modelling package," *J. Synchrotron Radiat.* **18**, 708–716 (2011).
14. X. Shi et al., "X-ray optics simulation and beamline design using a hybrid method: diffraction-limited focusing mirrors," *Proc. SPIE* **9209**, 920909 (2014).
15. F. Schaefers, "RAY—the BESSY raytrace program to calculate synchrotron radiation beamlines," 1996, https://www.helmholtz-berlin.de/media/media/grossgeraete/nanometeroptik/INT-Seminar/2011-06-29_-_ray.pdf (11 January 2014).
16. F. Schäfers, "The BESSY ray trace program to calculate (not only) synchrotron radiation beamlines," http://www.esrf.eu/files/live/sites/www/files/events/conferences/SMEXOS/talkSchaefers.pdf (26 January 2015).

17. F. Schäfers, "The BESSY raytrace program RAY," in *Modern Developments in X-Ray and Neutron Optics*, A. Erko et al., Eds., pp. 9–42, Springer, New York (2008).
18. E. Knudsen et al., "McXtrace: a Monte Carlo software package for simulating X-ray optics, beamlines and experiments," *J. Appl. Crystallogr.* **46**, 679–696 (2013).
19. E. Knudsen et al., "Novel applications of the x-ray tracing software package McXtrace," *Proc. SPIE* **9209**, 92090B (2014).
20. E. L. Church, H. A. Jenkinson, and J. M. Zavada, "Relationship between surface scattering and micro-topographic features," *Opt. Eng.* **18**(2), 125–136 (1979).
21. E. L. Church and H. C. Berry, "Spectral analysis of the finish of polished optical surfaces," *Wear* **83**, 189–201 (1982).
22. E. L. Church, "Statistical effects in the measurement and characterization of smooth scattering surfaces," *Proc. SPIE* **511**, 18–22 (1985).
23. E. L. Church and P. Z. Takacs, "Specification of surface figure and finish in terms of system performance," *Appl. Opt.* **32**(19), 3344–3353 (1993).
24. E. L. Church and P. Z. Takacs, "Specification of glancing- and normal-incidence x-ray mirrors," *Opt. Eng.* **34**(2), 353–360 (1995).
25. J. C. Stover, *Optical Scattering*, 2nd ed., SPIE Press, Bellingham, WA (1995).
26. D. Attwood, *Soft X-Rays and Extreme Ultraviolet Radiation*, Cambridge University Press, New York (1999).
27. H. Yamaoka et al., "Development and surface evaluation of large SiC x-ray mirrors for high-brilliance synchrotron radiation," *Japan. J. Appl. Phys.* **33**, 6718–6726 (1994).
28. J. Sherrington and G. W. Howarth, "Approximate numerical models of 3D surface topography generated using sparse frequency domain descriptions," *Int. J. Mach. Tools Manufact.* **38**(5–6), 599–606 (1998).
29. D. Spiga, "Analytical evaluation of the x-ray scattering contribution to imaging degradation in grazing-incidence x-ray telescopes," *Astron. Astrophys.* **468**, 775–784 (2007).
30. E. Sidick, "Power spectral density specification and analysis of large optical surfaces," *Proc. SPIE* **7390**, 73900L (2009).
31. E. L. Church, "Fractal surface finish," *Appl. Opt.* **27**(08), 1518–1526 (1988).
32. B. B. Mandelbrot, *The Fractal Geometry of Nature*, Freeman, San Francisco (1977).
33. V. V. Yashchuk et al., "Two dimensional power spectral density measurements of x-ray optics with the MicroMap interferometric microscope," *Proc. SPIE* **5858**, 58580A (2005).
34. V. V. Yashchuk et al., "Cross-check of different techniques for two dimensional power spectral density measurements of x-ray optics," *Proc. SPIE* **5921**, 59210G (2005).
35. V. V. Yashchuk et al., "Surface roughness of stainless-steel mirrors for focusing soft x-rays," *Appl. Opt.* **45**(20), 4833–4842 (2006).
36. V. V. Yashchuk et al., "21st century metrology for synchrotron radiation optics—understanding how to specify and characterize optics," in *3rd Int. Workshop on Metrology for X-ray Optics*, Satellite to SRI 2006, Pohang Accelerator Laboratory, Daegu, Korea (2006).
37. P. Z. Takacs et al., "2D spatial frequency considerations in comparing 1D power spectral density measurements," presented at *Optical Fabrication and Testing*, paper OWE5, Optical Society of America, Jackson Hole, Wyoming (13–17 June 2010).
38. Y. V. Yashchuk and V. V. Yashchuk, "Reliable before-fabrication forecasting of expected surface slope distributions for x-ray optics," *Opt. Eng.* **51**(4), 046501 (2012).
39. Y. V. Yashchuk and V. V. Yashchuk, "Reliable before-fabrication forecasting of expected surface slope distributions for x-ray optics," *Proc. SPIE* **8141**, 81410N (2011).
40. J. A. Ogilvy, *Theory of Wave Scattering from Random Rough Surfaces*, IOP Publishing Ltd., Bristol (1992).
41. I. V. Kozhevnikov, "General laws of x-ray reflection from rough surfaces: II. Conformal roughness," *Crystallogr. Rep.* **57**(04), 490–498 (2012).
42. S. M. Kay, *Modern Spectral Estimation: Theory and Application*, Prentice Hall, Englewood Cliffs (1988).
43. B. Murphy, "X-ray split and delay mirrors specifications," Drawings PF-391-946-11 and SA-391-946-13, LCLS, Menlo Park (2011).
44. V. V. Yashchuk et al., "Sub-microradian surface slope metrology with the ALS developmental long trace profiler," *Nucl. Instrum. Methods Phys. Res. A* **616**(2–3), 212–223 (2010).
45. V. V. Yashchuk et al., "A new x-ray optics laboratory (XROL) at the ALS: mission, arrangement, metrology capabilities, performance, and future plans," *Proc. SPIE* **9206**, 92060I (2014).
46. V. V. Yashchuk et al., "Correlation analysis of surface slope metrology measurements of high quality x-ray optics," *Proc. SPIE* **8848**, 88480I (2013).
47. D. J. Merthe, N. A. Artemiev, and V. V. Yashchuk, "Surface slope measurements of LCLS splitting mirror with the ALS DLTP," Light Source Beamline Note LSBL-1161, Advanced Light Source, Berkeley (2013).
48. F. Siewert et al., "Investigations on the spatial resolution of autocollimator-based slope measuring profilers," *Nucl. Instrum. Methods Phys. Res. A* **710**, 42–47 (2013).
49. J. D. Schmidt, *Numerical Simulation of Optical Wave Propagation*, SPIE Press, Bellingham, WA (2010).
50. G. M. Jenkins and D. G. Watts, *Spectral Analysis and Its Applications.*, Fifth Printing, Emerson-Adams Press, Boca Raton (2007).
51. I. V. Kozhevnikov, "On wave scattering from a rough surface of finite sizes," *J. Surf. Invest. X-Ray, synchrotron Neutron Tech.* **14**, 1425–1432 (1999).
52. G. Rasigni et al., "Autoregressive process for characterizing statistically rough surfaces," *J. Opt. Soc. Am. A* **10**(06), 1257–1262 (1993).
53. B.-S. Chen, B.-K. Lee, and S.-C. Peng, "Maximum likelihood parameter estimation of F-ARIMA processes using the genetic algorithm in the frequency domain," *IEEE Trans. Signal Process.* **50**(09), 2208–2219 (2002).
54. S. Y. Chang and H.-C. Wu, "Novel fast computation algorithm of the second-order statistics for autoregressive moving-average processes," *IEEE Trans. Signal Process.* **57**(02), 526–535 (2009).
55. V. V. Yashchuk, Y. N. Tyurin, and A. Y. Tyurina, "Application of time-invariant linear filter approximation to parameterization of one- and two-dimensional surface metrology with high quality x-ray optics," *Proc. SPIE* **8848**, 88480H (2013).
56. V. V. Yashchuk, Y. N. Tyurin, and A. Y. Tyurina, "Application of the time-invariant linear filter approximation to parametrization of surface metrology with high quality x-ray optics," *Opt. Eng.* **53**(8), 084102 (2014).
57. A. Rommeveaux et al., "First report on a European round robin for slope measuring profilers," *Proc. SPIE* **5921**, 59210I (2005).
58. F. Siewert et al., "Global high-accuracy inter-comparison of slope measuring instruments," DP-086 in*CD Proc. of the AIP Conf. on Synchrotron Radiation Instrumentation, III Workshop on Optical Metrology*, Daegu, South Korea (2006).
59. "IHS EViews 8 software," http://www.eviews.com/home.html (26 January 2015).
60. IHS EViews 8 user's guide, Volumes I and II, IHS Global Inc., Irvine 2014, http://www.eviews.com/download/download.html (26 January 2015).
61. A. P. Mancuso et al., "Scientific instrument single particles, clusters, and biomolecules (SPB)," XFEL.EU Technical Report 1-232, European XFEL, Hamburg, Germany (2013).
62. M. Altarelli et al., "The European x-ray free-electron laser," Technical Design Report DESY 2006-097, DESY XFEL Project Group, Hamburg, Germany (2007).
63. O. Chubar et al., "Time-dependent FEL wavefront propagation calculations: Fourier optics approach," *Nucl. Instrum. Methods Phys. Res. A* **593**(1–2), 30–34 (2008).
64. A. Buzmakov, L. Samoylova, and O. Chubar, "WPG documentation. Release 0.14," 2014, https://media.readthedocs.org/pdf/wpg/latest/wpg.pdf.
65. L. Samoylova et al., "Requirements on hard x-ray grazing incidence optics for European XFEL: analysis and simulation of wavefront transformations," *Proc. SPIE* **7360**, 73600E5 (2009).
66. P. J. Brockwell and R. A. Davis, *Time Series: Theory and Methods*, 2nd ed., Springer, New York (2006).



**Valeriy V. Yashchuk** is leading the X-Ray Optics Laboratory at the Advanced Light Source, LBNL. He received his MS degree in physics from St. Petersburg State University, Russia, in 1979 and a PhD degree from St. Petersburg Nuclear Physics Institute, Russia, in 1995. He has authored more than 150 scientific publications in the fields of atomic physics, nonlinear optics, electro- and magneto-optics, experimental scientific methods and instrumentation, and optical metrology. He is a member of SPIE.

**Liubov V. Samoylova** is a physicist in the X-Ray Optics Group at the European X-Ray Free Electron Laser. She received a PhD in solid-state physics from A.V. Shubnikov Institute of Crystallography, Moscow, Russia, in 1996. She has authored over 40 scientific publications in the fields of x-ray dynamical diffraction, coherent x-ray optics, experimental methods, and instrumentation. Her current interest is focused on design and optimization of x-ray free electron laser beamlines.

**Igor V. Kozhevnikov** is a leading scientist at the Shubnikov Institute of Crystallography, Moscow, Russia. He received his MS degree in physics from the Lomonosov Moscow State University, Russia, in 1980, a PhD degree from the Lebedev Physical Institute, Moscow, Russia, in 1987, and a doctor (highest) degree from the Shubnikov Institute of Crystallography in 2014. He is the author of about 150 journal papers and has written two book chapters. His current research interests include x-ray, soft x-ray and EUV optics, and x-ray methods to study matter.